A VERTEX BASED MULTIGRID ALGORITHM FOR THREE DIMENSIONAL COMPRESSIBLE FLOW CALCULATIONS

by

Antony Jameson

August 1986

for the ASME Symposium on Numerical Methods

for Compressible Flow

Anaheim, December 1986

Abstract

A new multigrid method for the solution of the inviscid compressible flow equations is presented. The algorithm uses a finite volume formulation with the flow variables stored at the cell vertices, and a multi-stage time stepping scheme augmented by residual averaging. In calculations of transonic flow past a swept wing the method exhibits remarkably fast convergence.

1. Introduction

The purpose of this paper is to describe a recently developed multigrid method for the solution of the three dimensional Euler equations of inviscid compressible flow. The last decade has seen rapid developments in methods for solving the Euler equations [1-5]. Several multigrid methods have also been proposed [6-11]. The present method, which requires only some rather simple modifications to the basic time stepping algorithm for the solution of the Euler equations, has proved to be remarkably efficient in practice.

The underlying idea is to integrate the time dependent Euler equations until they reach a steady state. The problem is first reduced to a set of ordinary differential equations by subdividing the domain into polygonal or polyhedral cells, and writing the conservation laws in integral form for each cell. The resulting semi-discrete model can then be integrated in time by a variety of discrete time stepping schemes, either implicit or explicit. If one assumes that the optimal time step increases with the space interval, then one can anticipate a faster rate of convergence on a coarser grid. This motivates the concept of time stepping on multiple grids. The cells of the fine mesh can be amalgmated into larger cells which form a coarser mesh. In each coarse mesh cell the conservation laws

are then represented by summing the flux balances of its constituent fine mesh cells, with the result that the evolution on the coarse mesh is driven by the disequilibrium of the fine mesh equations. Finally, the corrections on the coarse mesh are interpolated back to the fine mesh. This process can be repeated through a sequence of meshes in each of which the mesh spacing is doubled from the previous mesh. If the time step is also doubled each time the process passes to a coarser mesh, then a four level multigrid cycle consisting of one step on each mesh represents a total advance

$$\Delta t + 2\Delta t + 4\Delta t + 8\Delta t = 15\Delta t,$$

where Δt is the step on the fine mesh. Further improvements in efficiency can be realized by the introduction of more complicated multigrid cycles in which more work is performed on the coarse grids. These gains are contingent upon ensuring the stability of the composite process, and preventing too much attrition of the convergence rate from the disturbances introduced by interpolation from coarser to finer grids.

The space and time discretization schemes are described in Sections 2 and 3. The multigrid procedure is described in Section 4, and a method of analyzing the scheme for a simple model problem is presented in Section 5. The initial application of the method has been to the calculation of transonic flow past a swept wing. This is an important problem because transonic flow is the principal operating regime for both commercial and military aircraft. Some results are presented in Section 6.

2. Space Discretization of the Euler Equations

Let p, ρ, u, v, w, E and H denote the pressure, density, Cartesian velocity components, total energy and total enthalpy. For a perfect gas

$$E = \frac{p}{(\gamma-1)\rho} + \frac{1}{2}(u^2 + v^2 + w^2) , \quad H = E + p/\rho$$

where γ is the ratio of specific heats. The Euler equations for flow of a compressible inviscid fluid can be written in integral form as

$$\frac{\partial}{\partial t}\iiint_{\Omega} w d\Omega + \iint_{\partial\Omega} \underline{F} \cdot d\underline{S} = 0 \qquad (2.1)$$

for a domain Ω with boundary $\partial\Omega$ and directed surface element $d\underline{S}$. Here w represents the conserved quantity and F is the corresponding flux. For mass conservation

$$w = \rho , \quad \underline{F} = (\rho u, \rho v, \rho w)$$

For conservation of momentum in the x direction

$$w = \rho u, \quad \underline{F} = (\rho u^2 + p , \rho uv, \rho uw)$$

with similar definitions for the y and z directions, and for energy conservation

$$w = \rho E, \quad \underline{F} = (\rho Hu, \rho Hv, \rho Hw)$$

If we divide the domain into a large number of small subdomains, we can use equation (2.1) to estimate the average rate of change of w

in each subdomain. This is an effective method to obtain discrete approximations to equation (2.1), which preserve its conservation form. In general the subdomains could be arbitrary, but it is convenient to use either distorted cubic or tetrahedral cells. Alternative discretizations may be obtained by storing sample values of the flow variables at either the cell centers [1] or the cell vertices [5]. The algorithm in the present work uses variables stored at the vertices of the cells of a rectilinear mesh. A control volume for each vertex is formed by taking the union of the cells meeting at that vertex. Equation (2.1) then takes the form

$$\frac{d}{dt} \left(\sum_k V_k \right) w + \sum_k Q_k = 0 \qquad (2.2)$$

where V_k and Q_k are the cell volume and flux balance for the kth cell in the control volume. The flux balance for a given cell is now approximated as

$$Q = \sum_\ell \underline{F}_\ell \cdot \underline{S}_\ell \qquad (2.3)$$

where $\underline{S}_\ell$ is the directed area of the ℓth face, and $\underline{F}_\ell$ is an estimate of the mean flux vector across that face. Fluxes across internal faces cancel when the sum $\sum_k Q_k$ is taken in equation (2.5), so that only the external faces of the control volume contribute to its flux balance. The flux balance at each vertex can be evaluated directly by summing either the flux balances of its constituent cells or the contributions of its faces. The flux across each face is estimated by a simple arithmetic average of the values of the flow variables at the four corners of each face.

The approximation (2.2) needs to be augmented by artificial dissipative terms for two reasons. First there is the possibility of undamped oscillatory modes. For example, a mode with values ± 1 alternately at odd and even points leads to a numerically evaluated flux balance of zero in every interior control volume. Although the boundary conditions may suppress such a mode in the steady state solution, the absence of damping at interior points may have an adverse effect on the rate of convergence to the steady state. The second reason for introducing dissipative terms is to allow the clean capture of shock waves and contact discontinuities without undesirable oscillations. Following the pioneering work of Godunov [12], a variety of dissipative and upwind schemes designed to have good shock capturing properties have been developed during the past decade [13-23]. The concept of total variation diminishing (TVD) schemes, introduced by Harten [18], has proved particularly useful as a guide to the design of non-oscillatory schemes for scalar conservation laws. First order accurate TVD schemes can be realized either by upwinding, or the introduction of dissipative terms with a large enough coefficient. These ideas may be extended to the treatment of a system such as the Euler equations by splitting the flux into components corresponding to the different characteristic speeds, and applying the upwind or TVD construction separately to each component.

The use of flux splitting allows precise matching of the

dissipative terms to introduce the minimum amount of dissipation needed to prevent oscillations. This in turn reduces the thickness of the numerical shock layer to the minimum attainable, one or two cells for a normal shock. In practice, however, it turns out that shock waves can be quite cleanly captured without flux splitting by using adaptive coefficients. The dissipation then has a low background level which is increased in the neighborhood of shock waves to a peak value proportional to the maximum local wave speed. The second difference of the pressure has been found to be an effective measure for this purpose. The dissipative terms are constructed in a similar manner for each dependent variable by introducing dissipative fluxes which preserve the conservation form. For a three dimensional rectilinear mesh the added terms have the form

$$d_{i+1/2,j,k} - d_{i-1/2,j,k} + d_{i,j+1/2,k} - d_{i,j-1/2,k} + d_{i,j,k+1/2} - d_{i,j,k-1/2} \tag{2.4}$$

These fluxes are constructed by blending first and third differences of the dependent variables. For example, the dissipative flux in the i direction for the mass equation is

$$d_{i+1/2,j,k} = R(\epsilon^{(2)} - \epsilon^{(4)} \delta_x^2)(\rho_{i+1,j,k} - \rho_{i,j,k}) \tag{2.5}$$

where δ_x^2 is the second difference operator, $\epsilon^{(2)}$ and $\epsilon^{(4)}$ are the adaptive coefficients, and R is a scaling factor proportional to an estimate of the maximum local wave speed. For an explicit scheme the local time step limit Δt^* is a measure of the time it takes for the fastest wave to cross a mesh interval, and R can accordingly by made

proportional to $1/\Delta t^*$. The coefficient $\epsilon^{(4)}$ provides the background dissipation in smooth parts of the flow, and can be used to improve the capability of the scheme to damp high frequency modes. Shock capturing is controlled by the coefficient $\epsilon^{(2)}$, which is made proportional to the normalized second difference of the pressure

$$\nu_{i,j,k} = \left| \frac{p_{i+1,j,k} - 2p_{i,j,k} + p_{i-1,j,k}}{p_{i+1,j,k} + 2p_{i,j,k} + p_{i-1,j,k}} \right|$$

in the adjacent cells.

Schemes constructed along these lines combine the advantages of simplicity and economy of computation, at the expense of an increase in thickness of the numerical shock layer to three or four cells. They have also proved robust in calculations over a wide range of Mach numbers (extending up to 20 in recent studies [24]).

3. Time Stepping Scheme

The discretization procedures of Section 2 lead to set of coupled ordinary differential equations, which can be written in the form

$$\frac{dw}{dt} + R(w) = 0 \qquad (3.1)$$

where w is the vector of the flow variables at the mesh points, and R(w) is the vector of the residuals. The residual at each vertex consists of the flux balance defined by equations (2.2) - (2.5) divided by the sum of the volumes of the cells meeting at that vertex. These equations are to be integrated to a steady state. Multi-stage time stepping schemes prove to be effective for this purpose and they can also readily be adapted to drive a multigrid procedure. In the numerical solution of ordinary differential equations multi-stage schemes are usually designed to give a high order of accuracy. Since the present objective is simply to obtain a steady state as rapidly as possible, the order of accuracy is not important. This allows the use of schemes selected purely for their properties of stability and damping. For this purpose it pays to distinguish the hyperbolic and parabolic parts stemming respectively from the convective and dissipative terms, and to treat them differently. This leads to a new class of hybrid multi-stage schemes.

Dropping the subscripts i,j the general m stage hybrid scheme to advance a time step Δt can be written as

$$\begin{aligned} w^{(0)} &= w^n \\ w^{(1)} &= w^{(0)} - \alpha_1 \Delta t\, R^{(0)} \\ &\cdots \\ w^{(m-1)} &= w^{(0)} - \alpha_{m-1} \Delta t\, R^{(m-2)} \\ w^{(m)} &= w^{(0)} - \Delta t\, R^{(m-1)} \\ w^{n+1} &= w^{(m)} \end{aligned} \tag{3.2}$$

where w^n and w^{n+1} are the values at the beginning and end of the time step, and the residual in the q+1st stage is evaluated as

$$R^{(q)} = \sum_{r=0}^{q} \left\{ \beta_{qr}\, Q(w^{(r)}) - \gamma_{qr}\, D(w^{(r)}) \right\} \tag{3.3}$$

subject to the consistency constraint that

$$\sum_{r=0}^{q} \beta_{qr} = \sum_{r=0}^{q} \gamma_{qr} = 1 \tag{3.4}$$

A useful insight into the behavior of these schemes can be gained by considering the model problem

$$u_t + u_x + \mu \Delta x^3\, u_{xxxx} = 0 \tag{3.5}$$

In the absence of the third order dissipative term this equation describes the propagation of a disturbance without distortion at unit speed. With centered differences the residual has the form

$$\begin{aligned} \Delta t R_j = {} & \frac{\lambda}{2} (u_{j+1} - u_{j-1}) \\ & + \lambda\mu (u_{j+2} - 4u_{j+1} + 6u_j - 4u_{j-1} + u_{j-2} \end{aligned} \tag{3.6}$$

where $\lambda = \Delta t/\Delta x$ is the Courant number. If we consider a Fourier mode $\hat{u} = e^{ipx}$ the discretization in space yields

$$\Delta t \frac{d\hat{u}}{dt} = z\hat{u}$$

where z is the Fourier symbol of the residual. Setting $\xi = p\Delta x$, this is

$$z = -\lambda i \sin\xi - 4\lambda\mu(1 - \cos\xi)^2 \qquad (3.7)$$

In the complex plane z describes an oval path as ξ ranges from $-\pi$ to π. A single step of the multistage scheme yields

$$\hat{u}^{n+1} = g(z)\hat{u}^n$$

where g(z) is the amplification factor. The stability region of the scheme is given by those values of z for which $g(z) \leq 1$. The maximum stability interval along the imaginary axis attainable by an m stage scheme is m-1. Schemes achieving this limit have been characterized by Kinmark [25].

The computational requirements of a multi-stage scheme can be substantially reduced by freezing the dissipative part of the residual at the value $D(w^{(0)})$ in all stages of the scheme, so that in the $(q+1)^{st}$ stage

$$R^{(q)} = \frac{1}{S}\left\{Q(w^{(q)}) - D(w^{(0)})\right\} \qquad (3.8)$$

The amplification factor can no longer be represented as a polynomial, but it can easily be calculated recursively. If the time stepping scheme is to be used in a multi-grid procedure it is important that it should be effective at damping high frequency modes. One can fairly easily devise three and four stage schemes in the class defined by

equation (3.8) which meet this requirement. An effective three stage scheme is given by the coefficients

$$\alpha_1 = .6, \qquad \alpha_2 = .6 \tag{3.9}$$

Its stability region is shown in Figure 1.

Additional flexibility is provided by a class of schemes in which the dissipative terms are evaluated twice. This may be used to make a further improvement in the high frequency damping properties, or else to extend the stability region along the real axis to allow more margin for the dissipation introduced by a TVD scheme. In this class of schemes

$$R^{(0)} = \frac{1}{S}\left\{Q(w^{(0)}) - D(w^{(0)})\right\}$$

and (3.10)

$$R^{(q)} = \frac{1}{S}\left\{Q(w^{(q)}) - \beta D(w^{(1)}) - (1-\beta)D(w^{(0)})\right\}, \quad q \geq 1$$

In the case of pure dissipation (Qw = 0), the amplification factor reduces to

$$g = 1 + z + \alpha_1\beta\, z^2$$

Thus if β is chosen such that $\alpha_1\beta = 1/4$, the stability region will contain a double zero at $z = -2$ on the real axis. A maximum stability interval of 8 can be attained along the real axis by choosing β such that $\alpha_1\beta = 1/8$. Figure 2 shows the stability region of a five stage scheme in this class with the coefficients

$$\alpha_1 = 1/4, \quad \alpha_2 = 1/6, \quad \alpha_3 = 3/8, \quad \alpha = 1/2, \quad \beta = 1 \tag{3.11}$$

This scheme attains a stability interval of 4 along both the imaginary and the real axes.

As it stands the maximum permissable time step is restricted by the stability limit on the Courant number. This restriction can be relaxed by replacing the residual at each point by a weighted average of the neighboring residuals. In a one dimensional case one might replace the residual R_i by the average

$$\bar{R}_i = \epsilon R_{i-1} + (1-2\epsilon)\, R_i + \epsilon R_{i+1}$$

at each stage of the scheme. This smooths the residuals and also increases the support of the scheme, thus relaxing the restriction on the time step imposed by the Courant Friedrichs Lewy condition. If $\epsilon \geq 1/4$, however, there are Fourier modes such that $\bar{R}_i = 0$ when $R_i \neq 0$. To avoid this restriction it is better to perform the averaging implicitly by setting

$$-\epsilon \bar{R}_{i-1} + (1 + 2\epsilon)\, \bar{R}_i - \epsilon \bar{R}_{i+1} = R_i \tag{3.12}$$

For an infinite interval this equation has the explicit solution

$$R_i = \frac{1-r}{1+r} \sum_{q=-\infty}^{\infty} r^{|q|}\, R_{i+q} \tag{3.13}$$

where

$$\epsilon = \frac{r}{(1-r)^2}, \quad r < 1 \tag{3.14}$$

Thus the effect of the implicit smoothing is to collect information from residuals at all points in the field, with an influence coefficient which decays by factor r at each additional mesh interval from the point of interest.

Consider the model problem (3.5). According to equation (3.10)

the Fourier symbol (3.7) will be replaced by

$$z = -\lambda \frac{i \sin \xi + 4\mu(1-\cos\xi)^2}{1 + 2\epsilon(1-\cos\xi)}$$

In the absence of dissipation one now finds that stability can be maintained for any Courant number λ, provided that the smoothing parameter satisfies the condition

$$\epsilon \geq \frac{1}{4} \left\{ \frac{\lambda^2}{\lambda^{*2}} - 1 \right\}$$

where λ^* is the stability limit of the unsmoothed scheme.

In the three dimensional case the implicit residual averaging is applied in product form

$$(1 - \epsilon_x \delta_x^2)\ (1 - \epsilon_y \delta_y^2)\ (1 - \epsilon_z \delta_z^2)\ \bar{R} = R \qquad (3.15)$$

where δ_x^2, δ_y^2 and δ_z^2 are second difference operators in the x , y and z directions, and ϵ_x , ϵ_y and ϵ_z are the corresponding smoothing parameters. In practice the best rate of convergence is usually obtained by using a value of λ about three times λ^*, and the smallest possible amount of smoothing to maintain stability.

4. Multigrid Time Stepping Scheme

The discrete equations (3.1) describe the local evolution of the system in the neighborhood of each mesh point. The underlying idea of a multigrid time stepping scheme is to transfer some of the task of tracking the evolution of the system to a sequence of successively coarser meshes. This has two advantages. First, the computational effort per time step is reduced on a coarser mesh. Second, the use of larger control volumes on the coarser grids tracks the evolution on a larger scale, with the consequence that global equilibrium can be more rapidly attained. In the case of an explicit time stepping scheme, this manifests itself through the possibility of using successively large time steps as the process passes to the coarser grids, without violating the stability bound.

In general one can conceive of a multigrid scheme using a sequence of independently generated coarser meshes which are not associated with each other in any structured way. It is convenient, however, to generate the coarser meshes by eliminating alternate points in each coordinate direction. This allows the formulation of simple rules for the transfer of data between grids. In order to give a precise description of the multigrid scheme subscripts will be used

to indicate the grid. Several transfer operations need to be defined. First the solution vector on grid k must be initialized as

$$w_k^{(0)} = T_{k,k-1}\, w_{k-1}$$

where w_{k-1} is the current value on grid k-1, and $T_{k,k-1}$ is a transfer operator. Next it is necessary to transfer a residual forcing function such that the solution on grid k is driven by the residuals calculated on grid k-1. This can be accomplished by setting

$$P_k = Q_{k,k-1}\, R_{k-1}(w_{k-1}) - R_k(w_k^{(0)})$$

where $Q_{k,k-1}$ is another transfer operator. Then $R_k(w_k)$ is replaced by $R_k(w_k) + P_k$ in the time stepping scheme. Thus, the multi-stage scheme defined by equation (3.2) is reformulated as

$$w_k^{(1)} = w_k^{(0)} - \alpha_1\, \Delta t_k\, (R_k^{(0)} + P_k)$$

$$\cdots$$

$$w_k^{(q+1)} = w_k^{(0)} - \alpha_{q+1}\, \Delta t_k\, (R_k^{(q)} + P_k)$$

$$\cdots$$

The result $w_k^{(m)}$ then provides the initial data for grid k+1. Finally the accumulated correction on grid k has to be transferred back to grid k-1. Let w_k^+ be the final value of w_k resulting from both the correction calculated in the time step on grid k and the correction transferred from grid k+1. Then one sets

$$w_{k-1}^+ = w_{k-1} + I_{k-1,k}(w_k^+ - w_k^{(0)})$$

where w_{k-1} is the solution on grid k-1 after the time step on grid k-1 and before the transfer from grid k, and $I_{k-1,k}$ is an interpolation operator.

The solution transfer rule is simply to set $w_k^{(0)}$ to w_{k-1} at the coincident mesh point in grid k-1. The residual transfer rule is a weighted sum over the 9 nearest points in two dimensions, or the 27 nearest points in three dimensions. The corresponding transfer operator $Q_{k,k-1}$ can be expressed as a product of summation operators in the coordinate directions. Let μ_x denote an averaging operator in the x direction:

$$(\mu_x\ R)_{i+1/2,j,k} = \frac{1}{2}(R_{i,j,k} + R_{i+1,j,k})$$

and

$$(\mu_x^2\ R)_{i,j,k} = \frac{1}{4}\ R_{i-1,j,k} + \frac{1}{2}\ R_{i,j,k} + \frac{1}{4}\ R_{i+1,j,k}$$

Then in the three dimensional case

$$Q_{k,k-1} \equiv 8\ \mu_x^2\ \mu_y^2\ \mu_z^2$$

The interpolation operator $I_{k-1,k}$ transfers the corrections at coincident mesh points, and fills in the corrections at intermediate points by bilinear or trilinear interpolation.

5. Analysis of the Multigrid Time Stepping Scheme

The analysis of multigrid schemes is complicated by the nonuniformity of the process. If a mesh point is common to two meshes then corrections can be directly transferred from the coarse to the fine mesh. On the other hand the correction at a point of the fine mesh which is not contained in the coarse mesh has to be interpolated from the corrections at neighboring points. It is proposed here to circumvent this difficulty by modeling the multigrid process as a combination of two processes. The first is a uniform process in which every mesh point is treated in the same way, and the second is a nonlinear filtering scheme which eliminates the data from alternate points. For the sake of simplicity the analysis will be restricted to a one dimensional model. It also proceeds on the assumption that each coarser mesh is produced by eliminating alternate points of the finer mesh, so that there exists a set of points which are common to all the meshes.

Figure 3(a) illustrates the data flow of a two level scheme in which grid 1 is the finer mesh and grid 2 is the coarser mesh. Suppose that the calculation is simulating an equation of the form

$$\frac{du_j}{dt} = R_j(u) \tag{5.1}$$

where u_j is the dependent variable at mesh point j of grid 1, and $R(u_j)$ is the residual. Here it will be convenient to use bracketed superscripts to indicate the grid level, and to reserve the use of subscripts for the indication of the location of the mesh point in the fine grid. Suppose that the points 0,2,4... are common to both meshes, while the points 1,3,5... are eliminated in grid 2. A simple multigrid scheme can be described as follows. On grid 1 u_j is updated by a correction

$$\delta u_j^{(1)} = - \Delta t^{(1)} \; f(R_j(u)) \tag{5.2}$$

where the function f depends on the time stepping scheme. On grid 2 corrections are calculated as

$$\delta u_j^{(2)} = -\Delta t^{(2)} \; f(R_j^{(2)}) \quad , \; j = 1,3,5... \tag{5.3}$$

where the residual $R_j^{(2)}$ is calculated by accumulating the residuals at the nearest neighbors after first allowing for the correction introduced on grid 1. For example,

$$R_j^{(2)} = \epsilon \; R_{j-1}^{+} + 2(1-\epsilon) \; R_j^{+} + \epsilon \; R_{j+1}^{+} \tag{5.4}$$

where the degree of spreading is controlled by the parameter ϵ, and

$$R_j^{+} = R_j(u + \delta u^{(1)}) \tag{5.5}$$

Then on interpolating the corrections on grid 2 back to grid 1, the total correction of the complete multigrid scheme is

$$\delta u_j = \delta u_j^{(1)} + \delta u_j^{(2)} \quad , \; j \text{ even}$$

$$\delta u_j = \delta u_j^{(1)} + \frac{1}{2} \left(\delta u_{j-1}^{(2)} + \delta u_{j+1}^{(2)}\right), \quad j \text{ odd}$$

This process can be broken down into two stages as illustrated in

Figure 3(b). First the corrections $\delta u_j^{(2)}$ are calculated for all points of grid 1 by formulas (5.3)-(5.5) for j both even and odd. In effect the two level process is now calculated uniformly on the original fine grid. In the second stage $\delta u_j^{(2)}$ is then replaced by

$$\delta \bar{u}_j^{(2)} = \delta u_j^{(2)} \quad , \quad j \text{ even}$$

$$\delta \bar{u}_j^{(2)} = \frac{1}{2} (\delta u_{j-1}^{(2)} + \delta u_{j+1}^{(2)}), \quad j \text{ odd}.$$

This nonlinear filtering process eliminates the need to calculate $\delta u_j^{(2)}$ at the odd points, allowing these calculations to be shifted to a coarser grid. It introduces an additional error

$$e_j = 0 \quad , \ j \text{ even}$$
$$e_j = \frac{1}{2} (\delta u_{j-1}^{(2)} - 2\delta u_j^{(2)} + \delta u_{j+1}^{(2)}), \quad j \text{ odd}$$

Assuming the mesh to be uniform, this can be written as

$$e_j = \frac{1}{4} (\delta u_{j-1}^{(2)} - 2\delta u_j^{(2)} + \delta u_{j+1}^{(2)})(1 - \cos\frac{\pi}{\Delta x} x_j) \qquad (5.6)$$

where Δx is the mesh interval of the fine mesh, and $x_j = j\Delta x$ are its mesh points. Thus the filter introduces additional errors in the form of a carrier wave at the mesh frequency $\pi/\Delta x$ of the fine mesh, modulated by the second difference of the corrections $\delta u_j^{(2)}$ which would be calculated in the second stage of the uniform scheme. If we make the usual assumptions of linearity and periodicity, the multilevel uniform scheme can be analyzed by the Fourier method. If the multilevel uniform scheme is unstable, we can anticipate that the corresponding multigrid scheme will be unsound. Because of the injection of additional errors at various mesh frequencies by the interpolation process of the multigrid scheme, a reasonable criterion

is to require the multilevel uniform scheme to have a substantial stability margin at the mesh frequencies of all the meshes above the coarsest mesh in the sequence.

The following paragraphs address the question of the stability of the multilevel uniform scheme. The analysis is carried out for an initial value problem on an infinite interval governed by an equation of the form

$$\frac{\partial v}{\partial t} + Av = 0 \tag{5.7}$$

where A is a linear differential operator in one space dimension. The operator A may contain a forcing term, so that v is not zero when the system reaches a steady state. Let the vector u with elements u_j represent the discrete solution. The residual is

$$R = Pu \tag{5.8}$$

where P is a difference operator approximating Δt A. In the case of a pth order accurate scheme, if P is applied to the values $v_j = v(x_j)$ of the exact solution, then

$$Pv = \Delta t(Av + O(\Delta x)^p)$$

Using supercripts to denote the time steps,

$$u^{n+1} = u^n + \delta u$$

where the correction δu depends on the residual through the action of a time stepping operator F, corresponding to equation (5.2). For example, if we use the multi-stage scheme

$$
\begin{aligned}
u^{(0)} &= u^n \\
u^{(1)} &= u^{(0)} - \alpha_1 \, Pu^{(0)} \\
u^{(2)} &= u^{(0)} - \alpha_2 \, Pu^{(1)} \\
u^{(3)} &= u^{(0)} - \alpha_3 \, Pu^{(2)} \\
u^{n+1} &= u^{(3)}
\end{aligned}
$$

we find that

$$u^{(3)} = u^{(0)} - \alpha_3(I - \alpha_2 P + \alpha_2\alpha_1 P^2) \, Pu^{(0)}$$

Consequently

$$F = \alpha_3(I - \alpha_2 P + \alpha_2\alpha_1 P^2)$$

If we set

$$\hat{u}(\xi) = \Delta x \sum_{-\infty}^{\infty} u_j \, e^{-i\xi x_J/\Delta x}$$

then the Fourier transform of the residual (5.8) is $\hat{P}\hat{u}$ where $\hat{P}(\xi)$ is the Fourier symbol of the difference operator. Suppose, for example, that we consider the model problem (3.5) for which

$$A \equiv \frac{\partial}{\partial x} - \mu \, \Delta \, x^3 \, \frac{\partial^4}{\partial x^4}$$

and that we use the central difference scheme (3.6). Then

$$\hat{P}(\xi) = \lambda \, i \sin \xi + 4\lambda\mu(1 - \cos\xi)^2 \qquad (5.9)$$

Similarly if $\hat{F}(\xi)$ is the Fourier symbol of the time stepping operator,

then

$$\hat{\delta u}(\xi) = \hat{F}(\xi)\ \hat{P}(\xi)\ \hat{u}^n(\xi)$$

and

$$\hat{u}^{n+1}(\xi) = g(\xi)\ \hat{u}^n(\xi) \tag{5.10}$$

where $g(\xi)$ is the amplification factor

$$g(\xi) = I - \hat{F}(\xi)\ \hat{P}(\xi) \_ \tag{5.11}$$

Suppose that we have a nested set of grids with successively doubled mesh intervals. It is now convenient to revert to denoting the grids by subscripts 1,2,3... (Since the individual elements of the solution vector do not appear in the analysis this leads to no confusion). Consider a multigrid time stepping scheme in which time steps are taken on successive grids sequentially down to the coarsest grid, and the cycle is then repeated. In order to produce the same final steady state as a scheme using only the fine grid, the evolution on every grid except grid 1 should driven by the residuals calculated on the next finer grid. Let R_1^+ be the residual on grid 1 after the change δu_1, and let R_2 be the residual calculated on grid 2. Also let Q_{21} be the operator transferring residuals from grid 1 to grid 2, so that $Q_{21}\ R_1$ is a weighted sum of fine grid residuals corresponding to the coarse grid residual R_2. Then on grid 2 replace R_2 by

$$\bar{R}_2 = R_2 + S_2$$

where

$$S_2 = Q_{21}\ R_1^+ - R_2$$

and on grid 3 replace R_3 by

$$\bar{R}_3 = R_3 + S_3$$

where

$$\begin{aligned} S_3 &= Q_{32}(R_2^+ + S_2) - R_3 \\ &= Q_{32}(Q_{21}\, R_1^+ + R_2^+ - R_2) - R_3 \end{aligned}$$

With a single stage time stepping scheme δu_2 is determined by substituting the corresponding fine grid residual $Q_{21}R_1^+$ for R_2, but R_2 needs to be calculated because $R_2^+ - R_2$ appears in S_3. With a multi-stage time stepping scheme R_2 would be recalculated several times while S_2 would be frozen at its initial value on grid 2. If we examine the action of an m stage scheme on one of the coarser grids, we have

$$u_k^{(0)} = u_{k-1}^+$$

$$u_k^{(1)} = u_k^{(0)} - \alpha_1\, Q_{k,k-1}\, R_{k-1}^+$$

$$u_k^{(2)} = u_k^{(0)} - \alpha_2(R_k^{(1)} + Q_{k,k-1}\, R_{k-1}^+ - R_k^{(0)})$$

$$\cdots$$

$$u_k^{(m)} = u_k^{(0)} - (R_k^{(m-1)} + Q_{k,k-1}\, R_{k-1}^+ - R_k^{(0)})$$

$$u_k^+ = u_k^{(m)}$$

Here in the second stage

$$\begin{aligned} R_k^{(1)} - R_k^{(0)} &= P_k(u_k^{(1)} - u_k^{(0)}) \\ &= -\alpha_1 P_k\, Q_{k,k-1}\, R_{k-1}^+ \end{aligned}$$

whence

$$u_k^{(2)} - u_k^{(0)} = - \alpha_2 (I - \alpha_1 P_k) Q_{k,k-1} R_{k-1}^+$$

Following through the remaining stages, we find that

$$\delta u_k = u_k^{(m)} - u_k^{(0)} = - F_k Q_{k,k-1} R_{k-1}^+ \qquad (5.12)$$

where F_k is the time stepping operator on grid k as it would appear for a single grid.

Now consider the evolution of all quantities in the multigrid process, assuming that it is uniformly applied at every mesh point of grid l. Suppose that the collection operators Q_{21}, Q_{32} all have the same generic form. On the fine grid denote this by Q, with corresponding Fourier symbol $\hat{Q}(\xi)$. For example, if

$$(QR)_j = \frac{1}{2} R_{j-1} + R_j + \frac{1}{2} R_{j+1}$$

then

$$\hat{Q}(\xi) = 1 + \cos\xi \qquad (5.13)$$

On grid l denote the Fourier symbols of the residual and time stepping operators by

$$p_l = \hat{P}(\xi), \quad f_l = \hat{F}(\xi) \qquad (5.14a)$$

and the symbol of the first collection operator by

$$q_{21} = \hat{Q}(\xi) \qquad (5.14b)$$

For a system of equations these symbols will be matrices. On the subsequent levels the corresponding symbols are

$$p_k = \hat{P}(2^{k-1}\xi), \quad f_k = \hat{F}(2^{k-1}\xi) \qquad (5.14c)$$

and

$$q_{k,k-1} = \hat{Q}(2^{k-1}\xi) \qquad (5.14d)$$

Now on the first grid

$$\hat{\delta u}_1 = - f_1 r_1$$

where r_1 is the Fourier transform of the residual

$$r_1 = p_1 \hat{u}_1$$

On subsequent grids it follows from equation (5.12) that

$$\hat{\delta u}_k = - f_k r_k$$

where

$$r_k = q_{k,k-1} \; r^+_{k-1}$$

Since the system is linear

$$r^+_{k-1} = r_{k-1} + p_{k-1} \; \hat{\delta u}_{k-1}$$

(but in general r^+_{k-1} is not equal to $p_{k-1} \; u^+_{k-1}$ when $k > 2$).

Substituting for $\hat{\delta u}_{k-1}$, we find that

$$r_k = q_{k,k-1}(I - p_{k-1} \; f_{k-1}) r_{k-1} \tag{5.15}$$

Finally for an m level scheme

$$\hat{u}^+_m = \hat{u}_1 - \sum_{k=1}^{m} f_k \; r_k \tag{5.16}$$

Equations (5.14)-(5.16) define the stability of the complete multi-level scheme. The formulas can easily be evaluated for any particular choices of residual operator, time stepping operator and collection operator with the aid of a computer program. Figures 4 and 5 show typical results for the dissipative central difference scheme (3.6), with the collection operator (5.13). Both results are for blended multi-stage time stepping schemes of the class defined by equations (3.2) and (3.3). Figure 4 shows the amplification factor of

a three stage scheme in which the dissipative terms are evaluated once, as defined by equations (3.8) and (3.9). The Courant number is 1.5. As the number of levels is increased the stability curve defined by the amplification factor is compressed to the left, retaining a large margin of stability at all high frequencies. Thus the scheme should be resistant to the injection of interpolation errors. Figure 5 shows the amplification factor of a five stage scheme in which the dissipative terms are evaluated twice as defined by equations (3.10) and (3.11). Residual averaging is also included with a coefficient of .75, and the Courant number is 7.5. Although the stability curve exhibits a bump, there is still a substantial margin of safety, and this scheme has proved very effective in practice.

This method of analysis, in which the multigrid process is regarded as a multilevel uniform process on a single grid, subject to the injection of additional interpolation errors, can easily be modified to allow for alternative multigrid strategies, including more complicated V and W cycles. Nor is it necessary to use the same time stepping and residual operators on every grid. It may pay, for example, to use a simplified lower order scheme on the coarse grids.

6. Transonic Flow Calculations For Swept Wings

This section presents the results of some calculations using the method described in Sections 2-4. The application is the calculation of transonic flow past a swept wing. The five stage time stepping scheme defined by equations (3.10) and (3.11) was used in conjunction with residual averaging. A W cycle, as illustrated in Figure 6, was used in the multigrid procedure. This was found to be slightly more efficient than a simple V cycle.

The mesh was of C type in streamwise vertical planes, generated by the introduction of sheared parabolic coordinates. This was accomplished by a two stage mapping procedure. The first stage introduces parabolic coordinates by the transformation

$$(\bar{X} + i\bar{Y})^2 = \{x - x_o(z) + i\ (y - y_o)\}/t(z)$$

$$\bar{Z} = z$$

where z is the spanwise coordinate, t(z) is a scaling factor which can be used to control the number of cells covering the wing, and $x_o(z)$ and $y_o(z)$ are the coordinates of a singular line lying just inside the leading edge. The effect of this transformation is to unwrap the wing to a shallow bump Y = S(X,Z). The second stage is a shearing transformation

$$X = X, \quad Y = Y - S(X,Z), \quad Z = Z$$

which maps the wing to the coordinate surface Y = 0. The mesh is then constructed by the reverse sequence of mappings from a rectangular grid in the X,Y,Z coordinate system. Meshes of this type contain badly distorted cells in the neighborhood of the singular line where it passes into the flowfield beyond the wing tip. These cells, which have a very high aspect ratio and a triangular cross section, present a severe test of the robustness of the multigrid scheme.

Figure 7 shows a typical result for the well known ONERA M6 wing at Mach number of .840 and a angle of attack of 3.06 degrees. The was computed on a mesh containing 96 cells in the chordwise direction, 16 cells in the direction normal to the wing, and 16 cells in the spanwise direction. The figure shows equi-Mach contours on the surface and in a vertical plane above the wing.* Tables 1-3 show convergence histories for calculations of this case on 96x16x16, 144x24x24, and 192x32x32 meshes. The result of a calculation using 20 cycles on a previous coarser mesh was used to provide the initial data for each of these calculations. The maximum feasible number of grid levels was used in the multigrid cycle, four in the first two cases,

---

*I am indebted to G. Volpe for the use of his graphics software to prepare this paper.

and five in the last. It can be seen that the convergence rate does not vary much with the number of mesh cells, varying between an average reduction per cycle of .80 and .83 in the density residual. In all three cases the lift coefficient is converged to within .1 percent in less than 20 cycles. Table 4 shows the convergence history for a flow with a smaller supersonic zone, at a Mach number of .700 and an angle of attack of 2.06^{o}. In this case the convergence rate is .785.

These calculations were performed on a Cray XMP 216 belonging to Cray Research. Each cycle on the 192x32x32 mesh takes just under 8 seconds. Thus a calculation with 20 multigrid cycles can be completed in 3 minutes. If a 96x16x16 mesh is used a calculation with 20 cycles takes about 1/2 minute. Thus the method might be used for interactive design calculations.

Table 1

Calculation of the flow past the ONERA M6 wing at Mach .840 and 3.06^{o} angle of attack on a 96x16x16 mesh using 4 grid levels

Cycle	Average $d\rho/dt$	Lift Coefficient	Drag Coefficient
1	.115	.30335	.02507
10	$.226\ 10^{-2}$	.31829	.01990
20	$.885\ 10^{-4}$	.31738	.01987
30	$.535\ 10^{-5}$	.31743	.01987
40	$.645\ 10^{-6}$	.31744	.01987
50	$.821\ 10^{-7}$	.31744	.01987
60	$.109\ 10^{-7}$	.31744	.01987
70	$.142\ 10^{-8}$	.31744	.01987
80	$.256\ 10^{-9}$	.31744	.01987
90	$.682\ 10^{-10}$	.31744	.01987
100	$.210\ 10^{-10}$	.31744	.01987

Average reduction of $d\rho/dt$ per multigrid cycle .797.

Table 2

Calculation of the flow past the ONERA M6 wing at Mach .840 and 3.06° angle of attack on a 144x24x24 mesh using 4 grid levels

Cycle	Average $d\rho/dt$	Lift Coefficient	Drag Coefficient
1	.180	.31496	.02023
10	$.590\ 10^{-2}$	.31937	.01691
20	$.437\ 10^{-3}$	.31953	.01700
30	$.783\ 10^{-4}$	.31948	.01698
40	$.821\ 10^{-5}$	.31947	.01698
50	$.149\ 10^{-5}$	.31947	.01698
60	$.233\ 10^{-6}$	.31947	.01698
70	$.381\ 10^{-7}$	.31947	.01698
80	$.131\ 10^{-7}$	.31947	.01698
90	$.633\ 10^{-8}$	.31947	.01698
100	$.383\ 10^{-8}$	.31947	.01698

Average reduction of $d\rho/dt$ per multigrid cycle .837.

Table 3

Calculation of the flow past the ONERA M6 wing at Mach .840 and 3.06^{o} angle of attack on a 192x32x32 mesh using 4 grid levels

Cycle	Average $d\rho/dt$	Lift Coefficient	Drag Coefficient
1	.114	.31778	.01778
10	$.446\ 10^{-2}$	.31826	.01597
20	$.167\ 10^{-2}$	.31762	.01566
30	$.262\ 10^{-3}$	.31746	.01567
40	$.626\ 10^{-4}$	.31747	.01567
50	$.101\ 10^{-4}$	.31747	.01567
60	$.185\ 10^{-5}$	.31747	.01567
70	$.357\ 10^{-6}$	.31747	.01567
80	$.720\ 10^{-7}$	.31747	.01567
90	$.151\ 10^{-7}$	.31747	.01567
100	$.320\ 10^{-8}$	.31747	.01567

Average reduction of $d\rho/dt$ per multigrid cycle .833.

Table 4

Calculation of the flow past the ONERA M6 wing at Mach .700 and 2.06° angle of attack on a 144x24x24 mesh using 4 grid levels

Cycle	Average $d\rho/dt$	Lift Coefficient	Drag Coefficient
1	.135	.18681	.00863
10	$.865\ 10^{-3}$	.17961	.00645
20	$.268\ 10^{-4}$	.17918	.00647
30	$.126\ 10^{-5}$	.17919	.00647
40	$.138\ 10^{-6}$	.17919	.00647
50	$.205\ 10^{-7}$	.17919	.00647
60	$.349\ 10^{-8}$	.17919	.00647
70	$.615\ 10^{-9}$	.17919	.00647
80	$.113\ 10^{-9}$	.17919	.00647
90	$.224\ 10^{-10}$	.17919	.00647
100	$.502\ 10^{-11}$	.17919	.00647

Average reduction of $d\rho/dt$ per multigrid cycle .785.

7. Conclusion

These results clearly establish the benefits of the multigrid technique for convergence acceleration. The computational efficiency of the present method reduces the cost of three-dimensional compressible flow calculations to the point where they can be routinely used as an aerodynamic design tool. The method has been implemented in a modular computer program, in which the flow solution module is essentially independent of the grid generator, requiring only the Cartesian coordinates of the grid points, and a definition of which surfaces are inner and outer boundaries at which solid wall or far field boundary conditions should be applied. Thus the same method can be applied to a variety of configurations by substituting alternative grid generators. Studies are presently being pursued of an extension to the Navier Stokes equations.

References

1. Jameson, A., Schmidt, W., and Turkel, E., "Numerical Solution of the Euler Equations by Finite Volume Methods Using Runge-Kutta Time Stepping Schemes", AIAA Paper 81-1259, AIAA 14th Fluid Dynamics and Plasma Dynamics Conference, Palo, Alto, 1981.

2. Jameson, Antony, and Baker, Timothy J., "Solution of the Euler Equations for Complex Configurations", Proc. AIAA 6th Computational Fluid Dynamics Conference, Danvers, 1983, pp. 293-302.

3. Pulliam, T.H., and Steger, J.L., "Recent Improvements in Efficiency, Accuracy and Convergence for Implicit Approximate Factorization Algorithms", AIAA Paper 85-0360, AIAA 23rd Aerospace Sciences Meeting, Reno, January 1985.

4. MacCormack, R.W., "Current Status of Numerical Solutions of the Navier-Stokes Equations", AIAA Paper 85-0032, AIAA 23rd Aerospace Sciences Meeting, Reno, January 1985.

5. Jameson, A., Baker, T.J., and Weatherill, N.P., "Calculation of Inviscid Transonic Flow Over a Complete Aircraft", AIAA Paper 86-0103, AIAA 24th Aerospace Sciences Meeting, Reno, January 1986.

6. Ni, Ron Ho., "A Multiple Grid Scheme for Solving the Euler Equations", AIAA Journal, Vol. 20, 1982, pp. 1565-1571.

7. Jameson, A., "Solution of the Euler Equations by a Multigrid Method", Applied Math. and Computation, Vol. 13, 1983, pp. 327-356.

8. Jameson, A., and Schmidt, W., "Recent Developments in Numerical Methods for Transonic Flows", Proc. 3rd International Conference on Finite Elements in Nonlinear Mechanics, FENOMECH 84, Stuttgart, 1984, edited by J. St. Doltsinis, North-Holland, 1985, pp. 467-493.

9. Hall, M.G., "Cell Vertex Multigrid Schemes for Solution of the Euler Equations", IMA Conference on Numerical Methods for Fluid Dynamics", Reading, April 1985.

10. Hemker, P.W., and Spekreijse, S.P., "Multigrid Solution of the Steady Euler Equations", Proc. Oberwolfach Meeting on Multigrid Methods, December 1984.

11. Anderson, W.K., Thomas, J.L., and Whitfield, D.L., "Multigrid Acceleration of the Flux Split Euler Equations", AIAA Paper 86-0105, AIAA 24th Aerospace Sciences Meeting, Reno, January 1986.

12. Godunov, S. K., "A Difference Method for the Numerical Calculation of Discontinous Solutions of Hydrodynamic Equations", Mat. Sbornik, 47, 1959, pp. 271-306, translated as JPRS 7225 by U.S. Dept. of Commerce, 1960.

13. Boris, J. P., and Book, D. L., "Flux Corrected Transport. 1. SHASTA, A Fluid Transport Algorithm that Works", J. Comp. Phys. Vol. 11, 1973, pp. 38-69.

14. Van Leer, B., "Towards the Ultimate Conservative Difference Scheme. II, Monotonicity and Conservation Combined in a Second Order Scheme," J. Comp. Phys. Vol. 14, 1974, pp. 361-370.

15. Steger, J. L., and Warming, R. F., "Flux Vector Splitting of the Inviscid Gas Dynamics Equations with Applications to Finite Difference Methods," J. Comp. Phys., Vol. 40, 1981, pp. 263-293.

16. Roe, P. L., "Approximate Riemann Solvers, Parameter Vectors, and Difference Schemes", J. Comp. Phys., Vol. 43, 1981, pp. 357-372.

17. Osher, S., and Solomon, F., "Upwind Difference Schemes for Hyperbolic Systems of Conservation Laws", Math. Comp., Vol. 38, 1982, pp. 339-374.

18. Harten, A., "High Resolution Schemes for Hyperbolic Conservation Laws", J. Comp. Phys., Vol. 49, 1983, pp. 357-393.

19. Osher, Stanley, and Chakravarthy, Sukumar, "High Resolution Schemes and the Entropy Condition", SIAM J. Num. Analysis, Vol. 21, 1984, pp. 955-984.

20. Sweby, P. K., "High Resolution Schemes Using Flux Limiters for Hyperbolic Conservation Laws", SIAM J. Num. Analysis, Vol. 21, 1984, pp. 995-1011.

21. Anderson, B.K., Thomas, J.L., and Van Leer, B., "A Comparison of Flux Vector Splittings for the Euler Equations", AIAA Paper 85-0122, AIAA 23rd Aerospace Sciences Meeting, Reno, January, 1984.

22. Yee, H.C., "On Symmetric and Upwind TVD Schemes", Proc. 6th GAMM Conference on Numerical Methods in Fluid Mechanics, Gottingen, September 1985.

23. Jameson, A., "A Nonoscillatory Shock Capturing Scheme Using Flux Limited Dissipation", Lectures in Applied Mathematics, Vol. 22, Part 1, Large Scale Computations in Fluid Mechanics, edited by B. E. Engquist, S. Osher and R.C.J. Sommerville, AMS, 1985, pp. 345-370.

24. Yoon, S., and Jameson, A., "An LU Implicit Scheme for High Speed Inlet Analysis, AIAA Paper 86-1520, AIAA/ASME/ASEE 22nd Joint Propulsion Conference, Huntsville, June 1986.

25. Kinmark, I.P.E., "One Step Integration Methods with Large Stability Limits for Hyperbolic Partial Differential Equations", Advances in Computer Methods for Partial Differential Equations, V, edited by R. Vichnevetsky and R.S. Stepleman, IMACS, 1984, pp. 345-349.

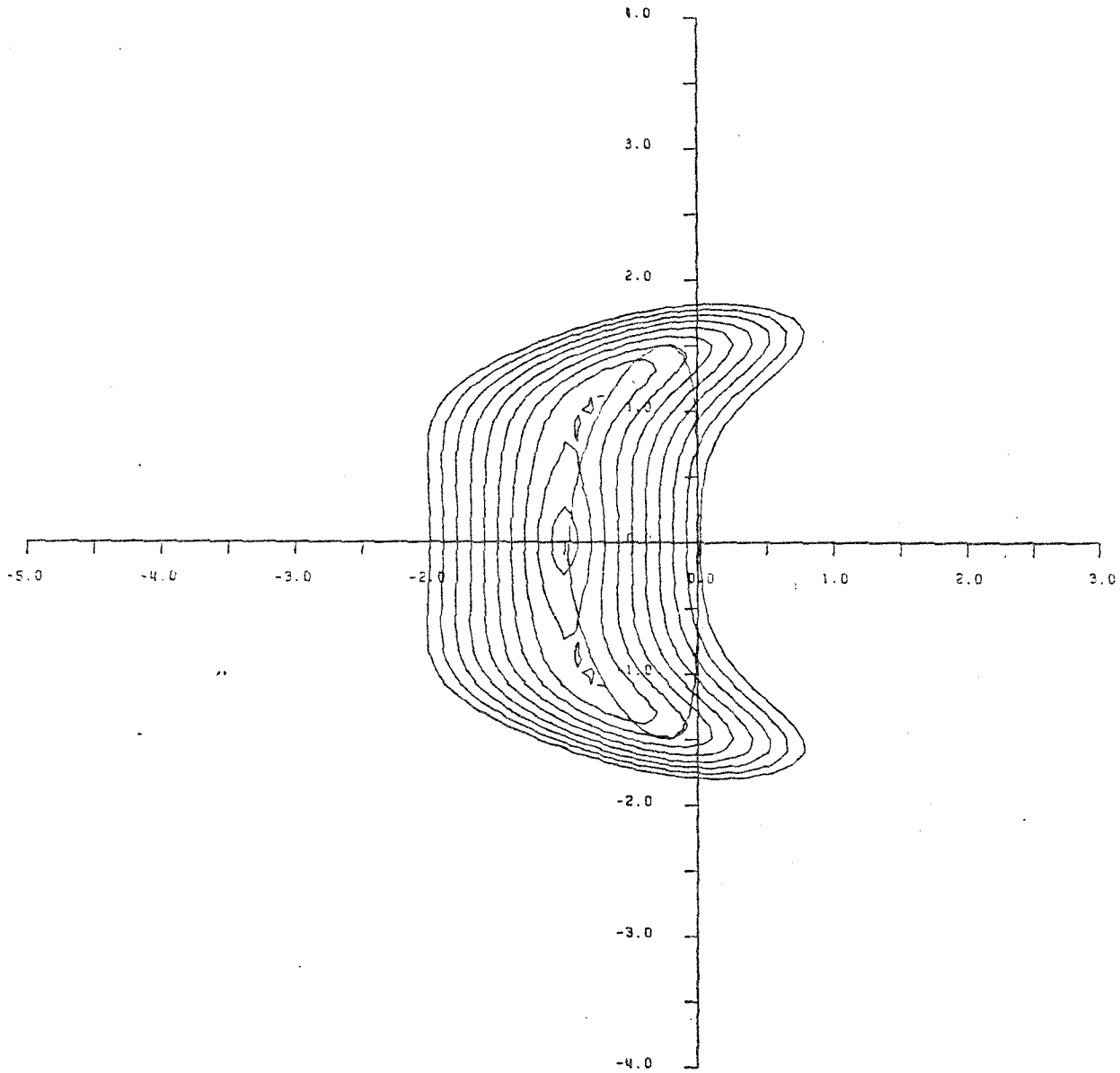

Figure 1

Stability region of 3 stage scheme with single evaluation of dissipation
Contour lines $|g| = 1., .9, .8, \ldots$
and locus of $z(\xi)$ for $\lambda = 1.5$, $\mu = .04$
Coefficients $\alpha_1 = .6$, $\alpha_2 = .6$

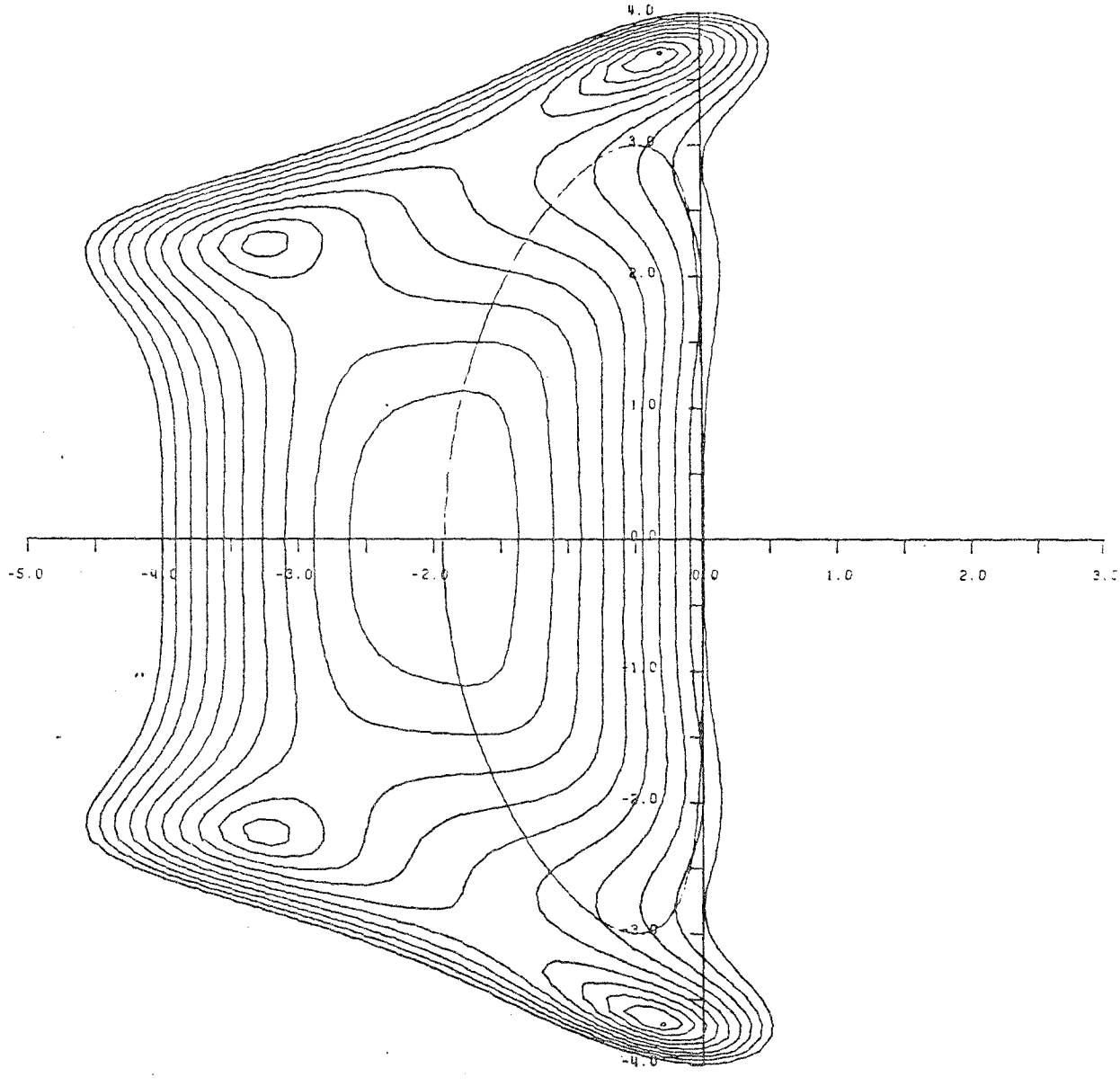

Figure 2

Stability region of 5 stage scheme with two evaluations of dissipation
Contour lines $|g| = .9, .8, .7, \ldots$
and locus of $z(\xi)$ for $\lambda = 3.$, $\mu = .04$
Coefficients $\alpha_1 = 1/4$, $\alpha_2 = 1/6$, $\alpha_3 = 3/8$, $\alpha_4 = 1/2$, $\beta = 1$

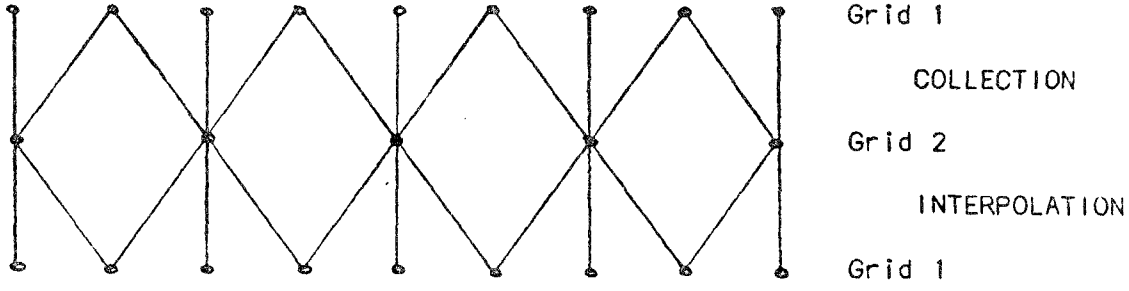

(a)

Multigrid scheme

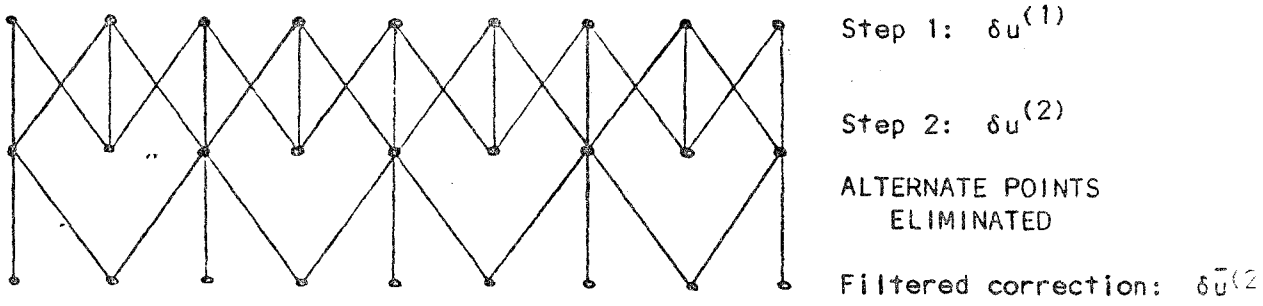

(b)

Uniform scheme with nonlinear filter

Figure 3

Data Flow of Multigrid and Uniform Schemes

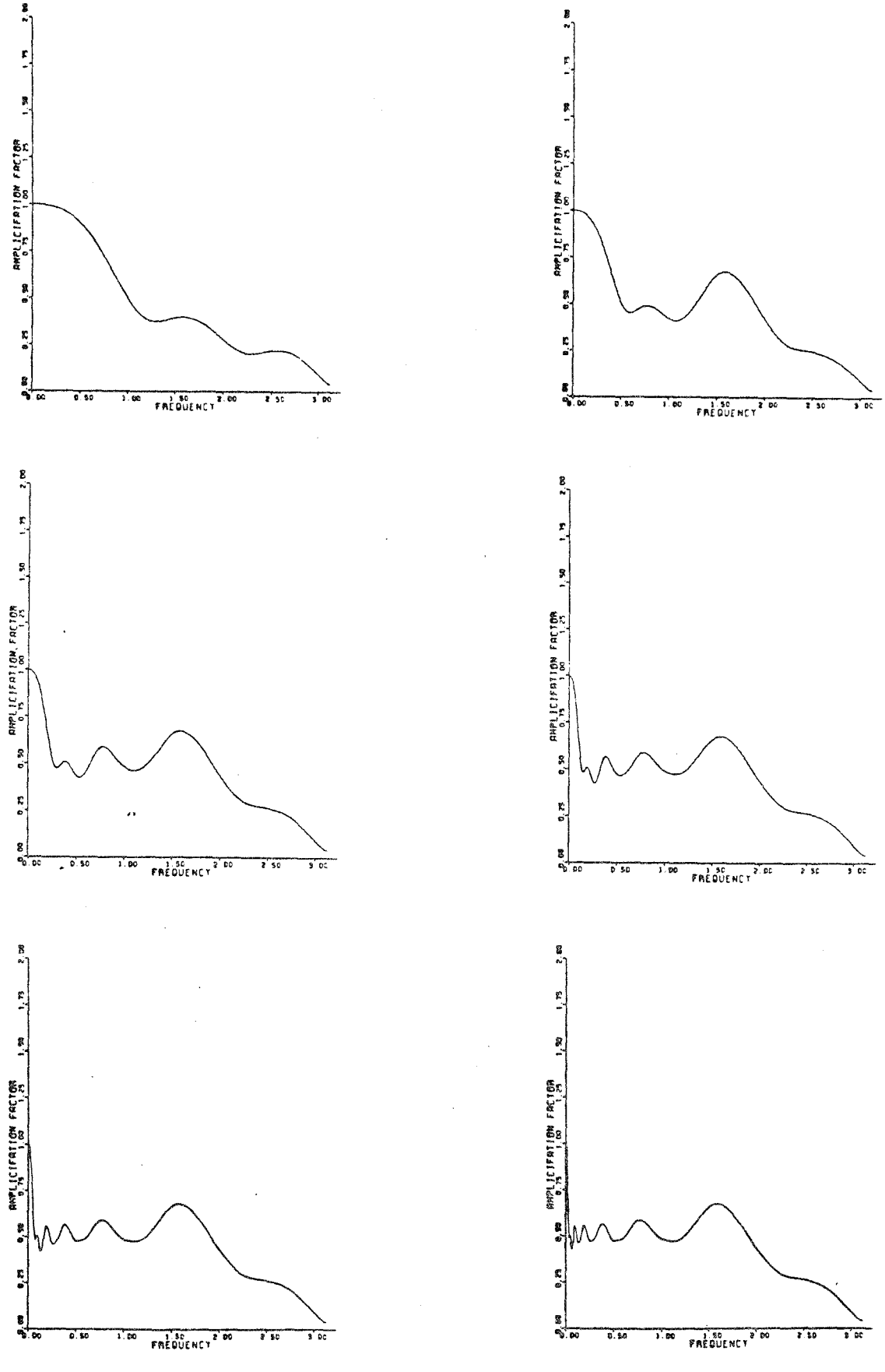

Figure 4

Amplification Diagrams for a 3 Stage Scheme
for 1-6 Grid Levels

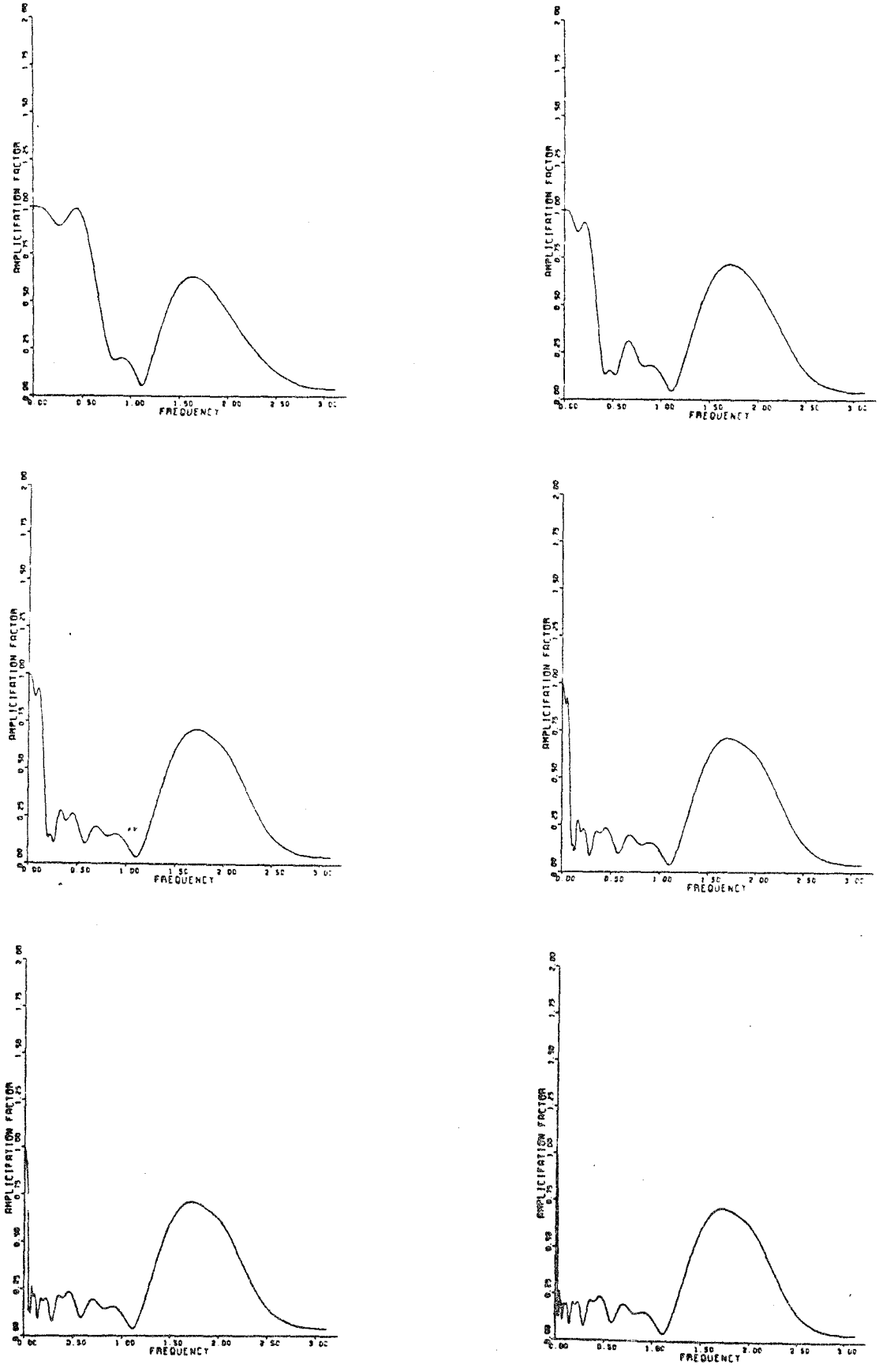

FIGURE 5

Amplification Diagrams for a 5 Stage Scheme
with 2 Evaluations of the Dissipative Terms
and Residual Averaging for 1-6 Grid Levels

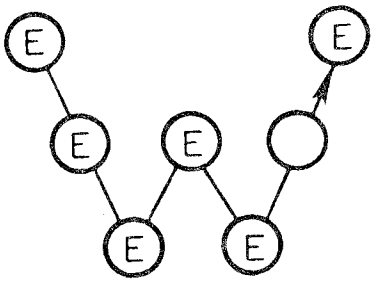

3 LEVELS
(a)

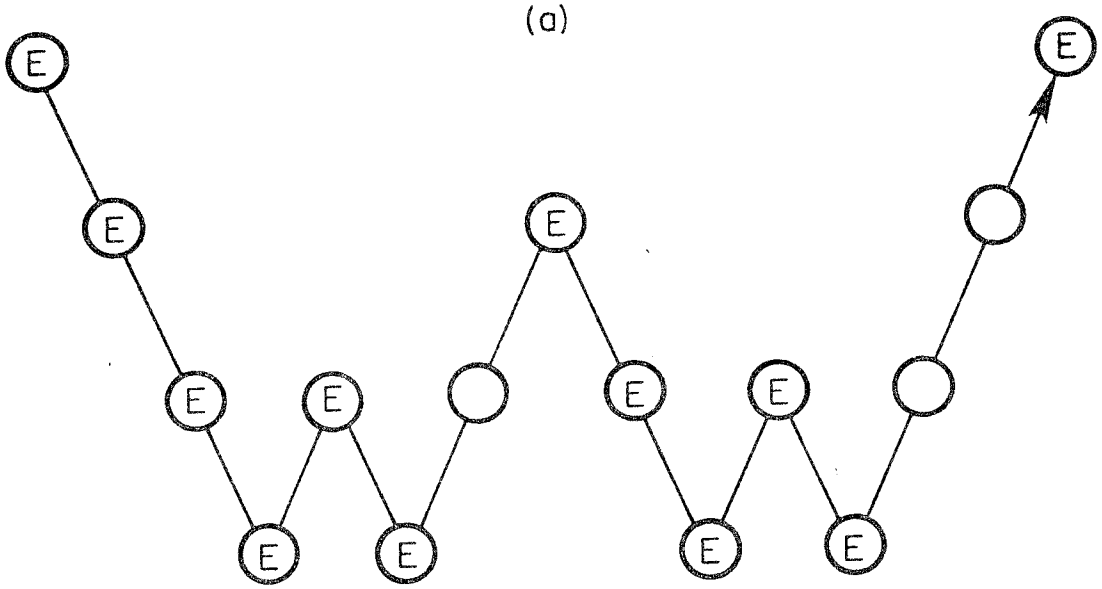

4 LEVELS
(b)

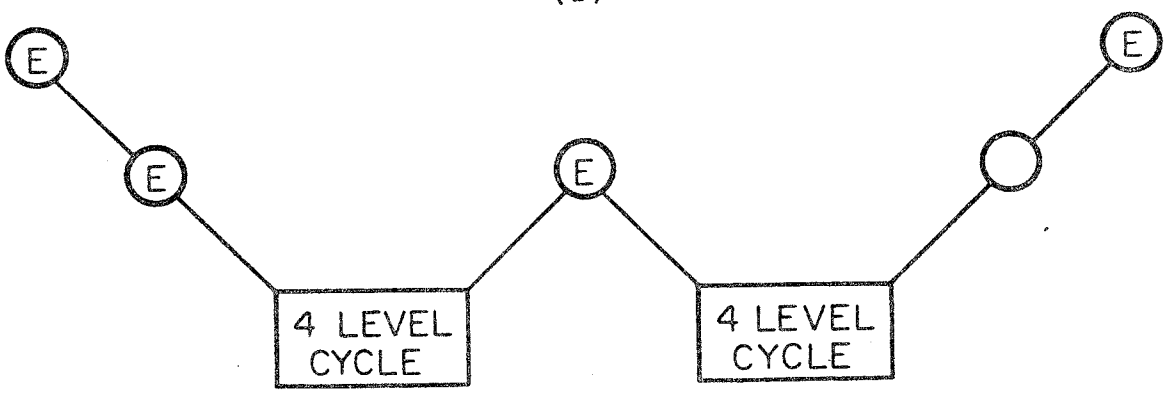

5 LEVELS
(c)

Figure 6

W cycle

E Calculate one time step

Transfer data without updating the solution.

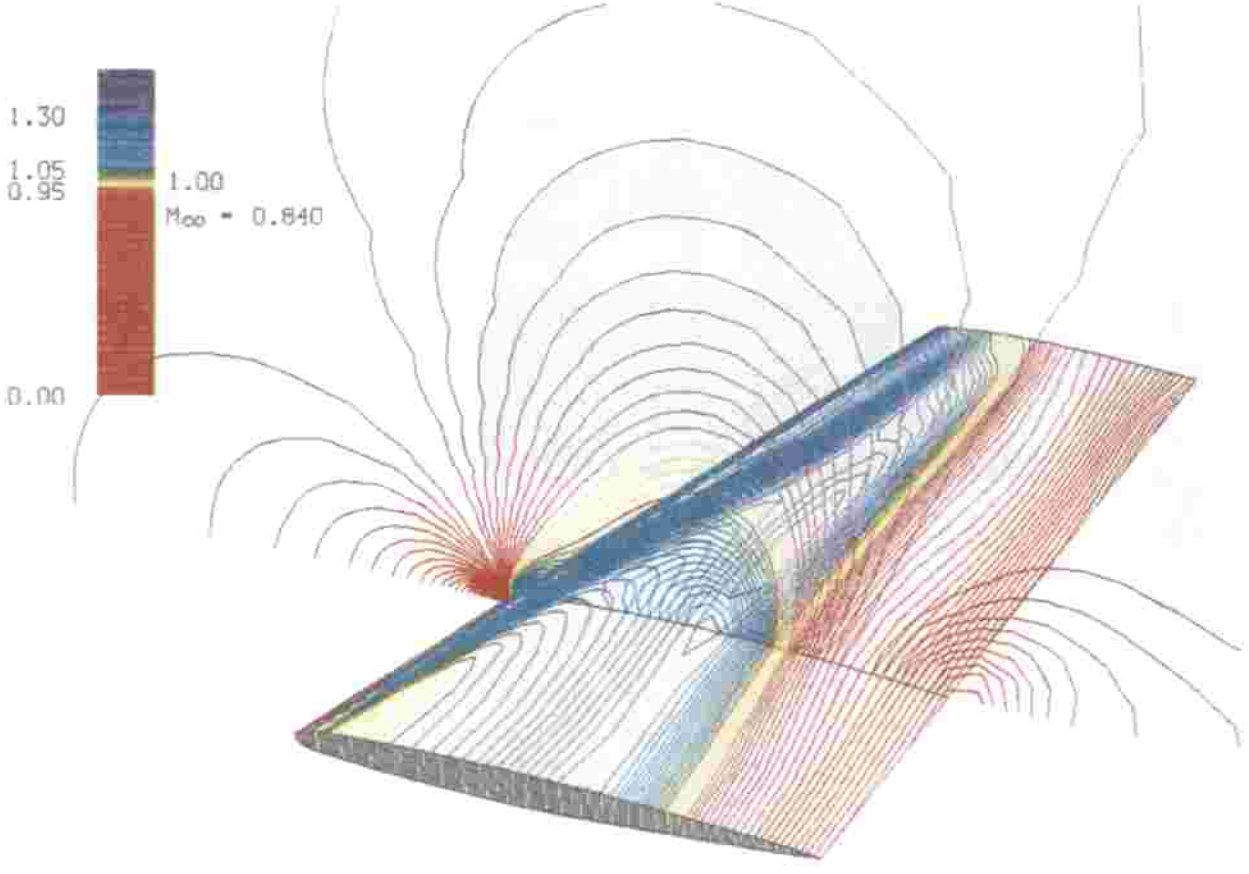

Figure 7

Constant pressure contours of flow over the ONERA M6 wing